Role of PCBM in the Suppression of Hysteresis in Perovskite Solar Cells

Yu Zhong, Martin Hufnagel, Mukundan Thelakkat, Cheng Li,* and Sven Huettner*

The power conversion efficiency of inorganic–organic hybrid lead halide perovskite solar cells (PSCs) is approaching that of those made from single crystalline silicon; however, they still experience problems such as hysteresis and photo/electrical-field-induced degradation. Evidences consistently show that ionic migration is critical for these detrimental behaviors, but direct in-situ studies are still lacking to elucidate the respective kinetics. Three different PSCs incorporating phenyl-C61-butyric acid methyl ester (PCBM) and a polymerized form (PPCBM) is fabricated to clarify the function of fullerenes towards ionic migration in perovskites: 1) single perovskite layer, 2) perovskite/PCBM bilayer, 3) perovskite/PPCBM bilayer, where the fullerene molecules are covalently linked to a polymer backbone impeding fullerene inter-diffusion. By employing wide-field photoluminescence imaging microscopy, the migration of iodine ions/vacancies under an external electrical field is studied. The polymerized PPCBM layer barely suppresses ionic migration, whereas PCBM readily does. Temperature-dependent chronoamperometric measurements demonstrate the reduction of activation energy with the aid of PCBM and X-ray photoemission spectroscopy (XPS) measurements show that PCBM molecules are viable to diffuse into the perovskite layer and passivate iodine related defects. This passivation significantly reduces iodine ions/vacancies, leading to a reduction of built-in field modulation and interfacial barriers.

1. Introduction

Driven by the demand for low cost and high-efficiency renewable energy sources, organometal trihalide perovskite (e.g., $CH_3NH_3PbI_3$ and $CH_3NH_3SnI_3$), first emerged as solar cells at 2009,[1] has attracted an unprecedented attention. Since then, extensive research has been carried out, ranging from crystalline structure characterization,[2] device performance optimization[3,4] to stability investigations,[5] etc. Though the surprising and remarkable progress has been achieved, perovskite solar cells (PSCs) are still suffering from several problems impeding a quick commercialization. Among those are the current density–voltage (J–V) hysteresis,[6,7] (the discrepancy of J–V curve between two sweeping directions)[8] or photo/electrical-induced degradation and stability,[9] for example. Recent evidences consistently demonstrate that ionic migration is responsible for these unsolicited behaviors.[10–14] The complexity of the investigation arises from the strong coupling between ionic migration and free charge carrier transport under external photo/electrical fields. Therefore, direct in situ characterization of the ionic movement via electrical and optical methods is becoming an emergent subject and will be used in this work.

It is widely observed that the involvement of phenyl-C61-butyric acid methyl ester (PCBM) molecules, either by mixing within the bulk,[15,16] or inserting a single layer into devices,[17,18] is able to significantly alleviate or eliminate hysteresis. Wojciechowski et al.[19] ascribed the reduced hysteresis to the enhanced electron transfer at the TiO_2/perovskite interface by a self-assembled monolayer of fullerenes. Xing et al.[20] observed the reduction of perovskite/TiO_2 interfacial barrier by inserting a PCBM layer. Shao et al.[17] attribute the elimination of hysteresis to the passivation of charge trap states in the bulk of perovskite film during the thermal annealing process. Xu et al.[15] found that the ion migration is significantly suppressed when PCBM are absorbed on Pb-I antisite defects. In this paper we will investigate the role of PCBM in detail. We utilize PCBM molecules as well as a polymerized form of PCBM molecules to corroborate their function, that is, investigate the influence of incorporation or interdiffusion, their function as an interlayer or a passivating agent. We intentionally used the typical organo-lead halide perovskite material ($CH_3NH_3PbI_{3-x}Cl_x$) with significant hysteresis. Very recent developments in perovskite solar cells often involve materials

Y. Zhong, Dr. C. Li, Dr. S. Huettner
Department of Chemistry
University of Bayreuth
Universitätstr. 30, Bayreuth 95440, Germany
E-mail: sven.huettner@uni-bayreuth.de
Dr. M. Hufnagel, Prof. M. Thelakkat
Applied Functional Polymers
University of Bayreuth
Universitätstr. 30, Bayreuth 95440, Germany
Prof. C. Li
School of Electronic Science and Engineering
Xiamen University
Xiamen 361005, China
E-mail: chengli@xmu.edu.cn

The ORCID identification number(s) for the author(s) of this article can be found under https://doi.org/10.1002/adfm.201908920.
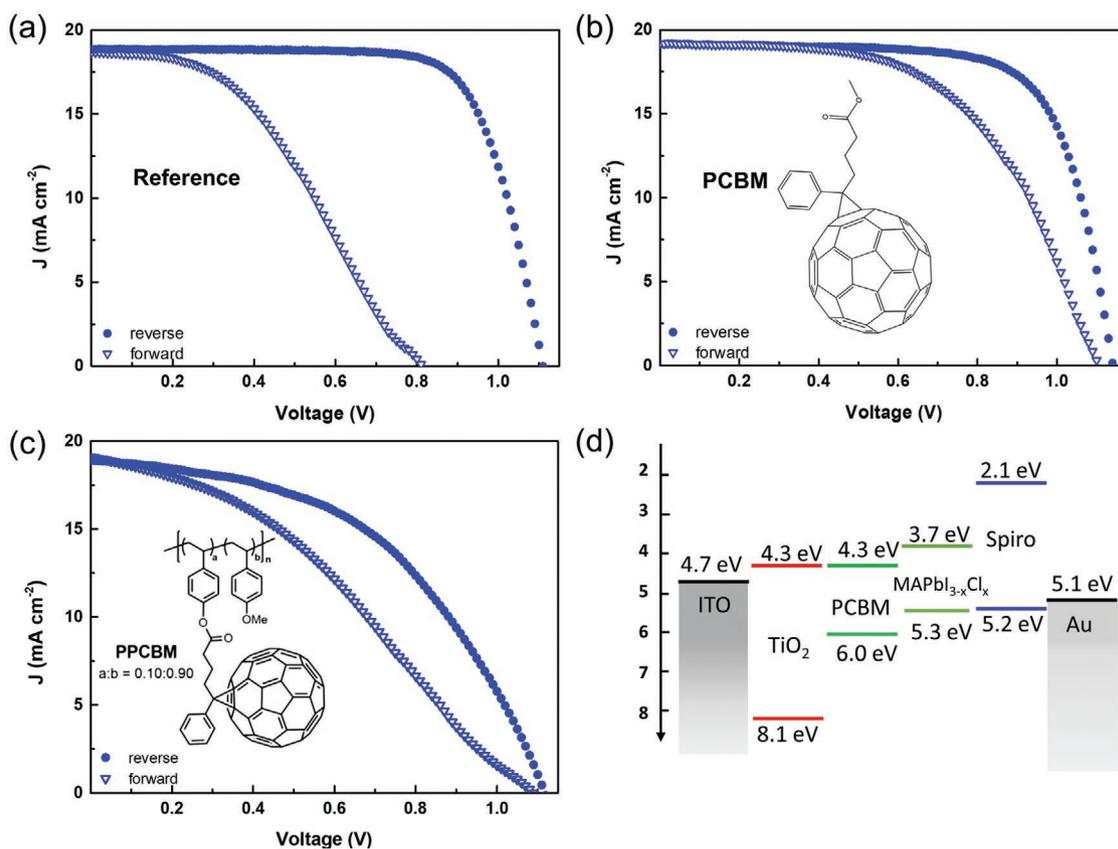
Figure 1. a–c) *J–V* curve characterization of different PSCs. a) Reference device, that is, FTO/compact TiO$_2$/perovskite/Spiro-OMeTAD/Au. b) Solar cells with a PCBM molecule layer, that is, FTO/compact TiO$_2$/PCBM/perovskite/Spiro-OMeTAD/Au. c) Solar cells with a PPCBM layer, that is, FTO/compact TiO$_2$/PPCBM/perovskite/Spiro-OMeTAD/Au. d) Energy diagram of the perovskite device. Insets in (b) and (c) are the chemical structure of PCBM molecule and PPCBM, respectively. The scanning speed is 0.8 V s^{-1}.

such as FAI[21] or 2D-perovskite[22] materials, where the hysteresis phenomena is not so obvious, which makes it more difficult to study the crucial role of PCBM on hysteresis suppression.

Wide-field photoluminescence (PL) imaging microscopy is employed to in situ study the motion of ions under an external electrical field in three individual systems: 1) single perovskite film 2) perovskite film deposited on top of a PCBM layer, called perovskite/PCBM bilayer 3) perovskite/PCBM-grafted polymer (PPCBM) bilayer. With this set of device structures we are able to identify the function of the PCBM layer and especially address its incorporation or interdiffusion and grain boundary passivation. Furthermore, we carry out the stepwise temperature dependent chronoamperometric measurements to obtain the activation energy of ion migration in PSCs, with and without PCBM layer respectively. X-ray photoemission spectroscopy (XPS) depth profiling indicates the incorporation or diffusion of PCBM molecules into the perovskite film, resulting in reduced ionic migration within perovskite layer. Therefore, PCBM can play an important role in the suppression of hysteresis by reducing ionic migration.

2. Results and Discussion

Figure 1a displays the *J–V* curve of a reference PSC using a mixed halide perovskite precursor (CH$_3$NH$_3$I:PbCl$_2$ = 3:1). Note

that in the reverse sweeping, from positive to negative voltage, as shown in **Table 1**, the efficiency is ≈15.5%, however, in the forward sweeping, from negative to positive voltage, the efficiency drops to 6.2%. When a PCBM layer is inserted between the perovskite and the TiO$_2$ electron transport layer (ETL), as shown in Figure 1b, the power conversion efficiency (η) of solar cells is comparable with the reference device in reverse scan direction. In forward scan direction, the PCBM-inserted devices yield a better performance, that is, fill factor (FF) and open-circuit voltage (V_{oc}), in comparison with that of the reference device. The photovoltaic parameters from a series of solar cells with and without PCBM are shown in Figure S1, Supporting Information. To quantitatively compare the hysteresis between the different solar cell structures, we utilize the so-called hysteresis index (HI). The HI is defined as[23,24]

$$ HI = \frac{J_{reverse}\left(\frac{V_{oc}}{2}\right) - J_{forward}\left(\frac{V_{oc}}{2}\right)}{J_{reverse}\left(\frac{V_{oc}}{2}\right)} \tag{1} $$

A solar cell without hysteresis yields an HI of 0, while a HI of 1 corresponds to a hysteresis as high as the magnitude of the photocurrent. The HIs are derived from the results in Figure 1 and listed in Table 1. The data imply that the hysteresis of

Table 1. Summary of device performance in Figure 1.

Device type	Scan direction	V_{oc} [V]	J_{sc} [mA cm^{-2}]	FF [%]	η [%]	Hysteresis Index
Reference	Forward	0.82	18.8	40.3	6.2	0.20
	Reverse	1.10	19.0	73.4	15.5	
PCBM layer	Forward	1.11	19.4	55.1	11.8	0.03
	Reverse	1.14	19.3	71.4	15.7	
PPCBM	Forward	1.10	19.1	35.1	7.4	0.19
	Reverse	1.11	19.0	48.7	10.4	

PCBM-incorporated devices significantly decreases compared with reference one.

To further study the role of the PCBM layer, we replace the PCBM layer with a polymerized PPCBM layer. The synthesis of this PPCBM is describe elsewhere.[25] This PPCBM has a molecular weight of $M_n = 17.2$ kg mol^{-1} and poly-dispersity of Đ = 1.27 (measured with size-exclusion chromatography with chlorobenzene as eluent and polystyrene calibration). Interestingly, the HI becomes large again with the utilization of this PPCBM. The HI approaches the value of the reference solar cell. In this PPCBM shown in inset of Figure 1c, PCBM molecules are bound to a polymer backbone and therefore immobilized within the polymer layer. This result implies that the diffusion of PCBM molecules into the perovskite layer is crucial to the elimination of hysteresis in PSCs, consistent with the requirement of thermal annealing to passivate the defects and decrease the trap density in the perovskite layer.[20] Here, we note that, the relatively poorer performance of the device with PPCBM is probably caused by its relatively lower electron mobility,[26] hindering the effective electron extraction by TiO$_2$/FTO layer.

Though various models for the J–V curve hysteresis have been proposed, including ferroelectricity,[27] charge trapping/detrapping,[28] modulated Schottky barriers[29] etc., it is supported by many evidences that a combination of ion migration[30,31] and polarization at interfaces[32,33] serves as an essential factor in the hysteretic behavior in PSCs. To study the ionic migration process, perovskite films with laterally-configured electrodes have demonstrated to be an excellent platform.[34,35] In addition, PL is an indication of the charge carrier recombination pathway[36] which has been employed to study the detailed charge carrier dynamic processes within the perovskite film.[37,38] Here, we investigate the dynamics of ion/vacancy migration with lateral interdigitating electrodes (Figure S3, Supporting Information) under an electrical field characterized by temporal-resolved PL imaging microscopy (Figure S4, Supporting Information), while the corresponding current is measured. The films were excited with blue light and their PL response > 700 nm was imaged. A detailed description of the setup has been reported previously.[39,40] In brief, we modified a commercial PL microscope and used a blue light excitation filter, dichroic mirror, and a fast charge-coupled device (CCD) camera to capture the PL response in wide field with high time resolution. PL images of the perovskite films were recorded while a fixed external electric field was applied laterally and its time-dependent current was measured.

Figure S5, Supporting Information depicts the temporal PL evolution of a perovskite film under a constant electrical field. It is observed that the overall PL intensity decreases after the injection of electrons. The reason is the formation of the quenching

defect when electrons are injected.[41] It has been observed that the defects, for example, Frenkel defects with iodine vacancies and interstitials,[42] formed during the low-temperature fabrication method,[43] can be driven by the external electrical field.[12,42] Our previous study showed that migrating iodine vacancies play a major role and migrate within the applied electric field. On their way towards the cathode, they partially compensate for interstitial defects but also leave behind a significant number of non-radiative recombination centers as their counterpart in Frenkel defects.[39] The migration of vacancies goes ahead with a decrease of the electron-hole concentration corresponding to an effective reduction p-doping density. This phenomenon is shown in Figure S5a–d, Supporting Information. A PL dark area expands from the positive side to negative side. As evidence of the reduction of electron–hole density (less p-type doping), the measured current decays, as displayed in Figure S5e, Supporting Information. Applying a dynamic model for the current within the device leads to the ionic mobility in perovskite reference samples $(2 \pm 1) \times 10^{-7}$ cm^2 V^{-1}s^{-1}.[39] The model used to determine the mobility is demonstrated in Section S6, Supporting Information.

Results were obtained for all three device structures, as illustrated in **Figure 2**. The ionic mobility of perovskite/PPCBM is $(1 \pm 1) \times 10^{-7}$ cm^2 V^{-1} s^{-1}, which is in similar range as the perovskite reference sample. The mobility of perovskite/PCBM system, however, is only $(4 \pm 2) \times 10^{-8}$ cm^2 V^{-1} s^{-1} almost one order of magnitude lower than that of the two other structures as illustrated in Figure 2. This shows that the ionic migration in perovskite films deposited on a PCBM layer is significantly
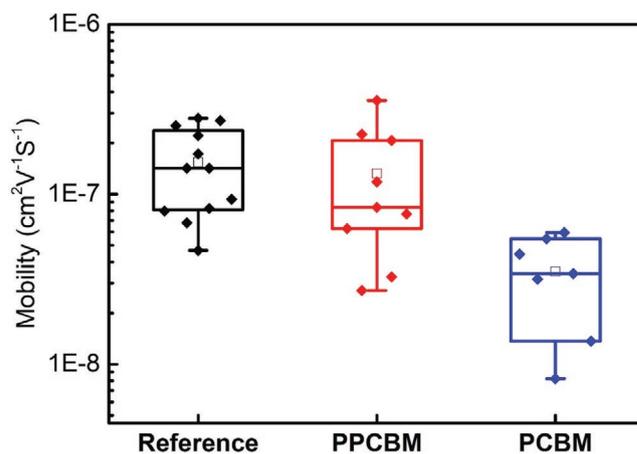

Figure 2. The ionic mobility in perovskite film. The results are derived from time-dependent current, as illustrated in Figure S5, Supporting Information.
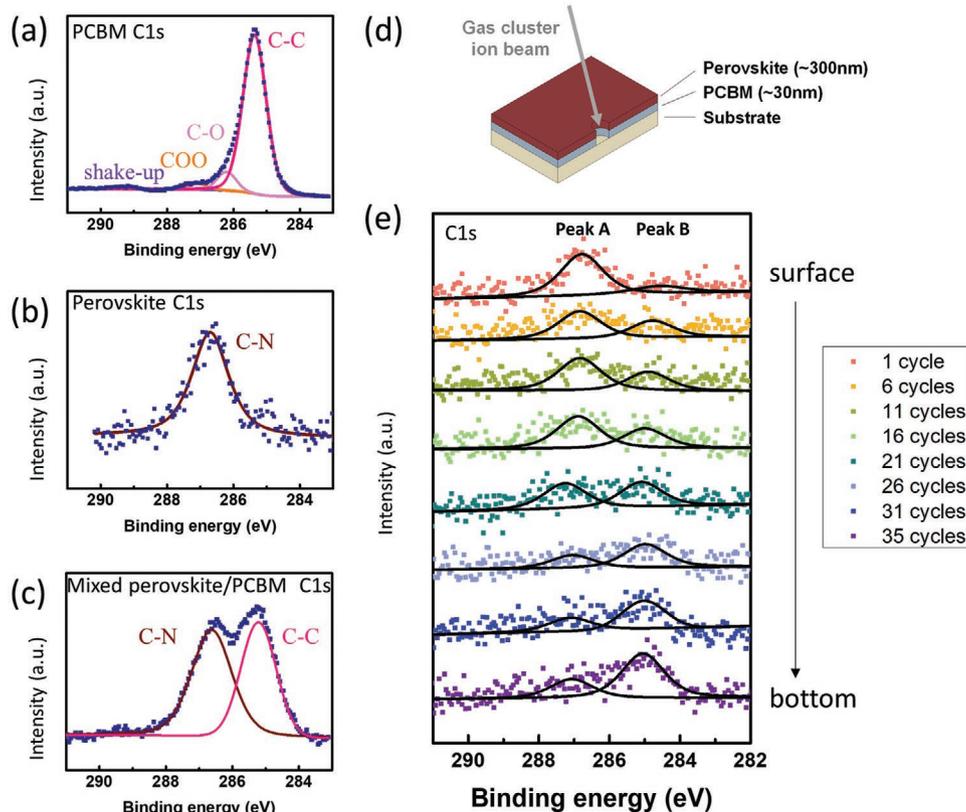
**ADVANCED
SCIENCE NEWS**

www.advancedsciencenews.com

**ADVANCED
FUNCTIONAL
MATERIALS**

www.afm-journal.de

Figure 3. XPS spectra of C1s peak on a) PCBM, b) perovskite, and c) perovskite/PCBM mixed sample. d) perovskite/PCBM bilayer sample for depth profile and e) its depth profile results after sputtering of gas cluster ion beam, where peaks A and B correspond to C1s from perovskite and PCBM respectively.

reduced compared to the pure perovskite film and the perovskite film on PPCBM. As we have mentioned above, the hysteresis is strongly related to the ionic migration in PSCs. Ions accumulate at the contacts on either side, with the ETL or hole transport layer (HTL), which will influence the built-in potential. Furthermore, a properly aligned built-in potential is favorable for charge injection and is also related to the maximum achievable V_{oc}.[30]

We find that PCBM which can freely interact or interdiffuse within a perovskite film decreases the ionic migration, and hence reduces the hysteresis in PCBM. In comparison, the glass transition temperature $T_g = 144\ °C$ of this PPCBM is above the processing temperature of the perovskite, the PPCBM layer does not allow any strong interdiffusion within the perovskite film.[25] Thus, the PCBM groups solely locate at the interface. The PSCs using a PPCBM layer between TiO_2 and perovskite still suffer severe hysteresis. This gives rise to the assumption that PCBM molecules indeed diffuse into perovskite films facilitating a passivating effect towards ionic migration. In order to corroborate our results, we analyzed the depth profile of a perovskite/PCBM bilayer sample with XPS in detail.

Figure 3a and b show the C1s spectra of a pure PCBM film and a pure perovskite film. PCBM shows a main peak at 285.3 eV, which originates from the C−C bond of the fullerene moiety.[44,45] The typical C1s signal of a perovskite film is the C−N feature of $CH_3NH_3^+$ (286.7 eV).[46,47] Furthermore, a third sample was processed, which was prepared by directly mixing the perovskite precursor solution with PCBM in a molar ratio

of Pb:PCBM = 500:1 and annealing. It is noted that the morphology of this intermixed film is sufficiently good to carry out our XPS analysis, but it does not allow the fabrication of proper solar cell devices. The C1s spectrum of this mixed perovskite/PCBM film (displayed in Figure 3c) is composed of two distinct peaks, which are ascribed to the C−N bond from perovskite and the C−C bond from PCBM. It indicates that the contribution of $CH_3NH_3PbI_{3-x}Cl_x$ and PCBM can be easily separated by analyzing the C1s peak. With this information we performed a depth profile of a perovskite/PCBM bilayer sample. A gas cluster ion beam (GCIB) was used to sputter into the organic film and to obtain a depth profile of the perovskite/PCBM bilayer sample, displayed in Figure 3d. The C1s spectrum obtained after every cycle (0.5 min per cycle) of GCIB sputtering is shown in Figure 3e. The sputter rate is ≈17 nm min^{-1} and after 18min-GCIB sputtering, the substrate surface was reached. It is obvious that through the perovskite layer two C1s peaks were detected. Peak A, at higher binding energy, which is ascribed to $CH_3NH_3^+$ from the perovskite, locates between 286.7 and 287.0 eV. This peak shifts to a lower position when it reaches the interface. This thickness-dependent shift has been reported.[46] The appearance of additional peaks formed by sputtering and beam damage have been excluded as shown in Figure S7, Supporting Information. Peak B, at around 285.3 eV, was also detected during the beginning cycles. Based on the results above, Peak B is attributed to the C−C bond stemming from PCBM, and shows their prevalence within
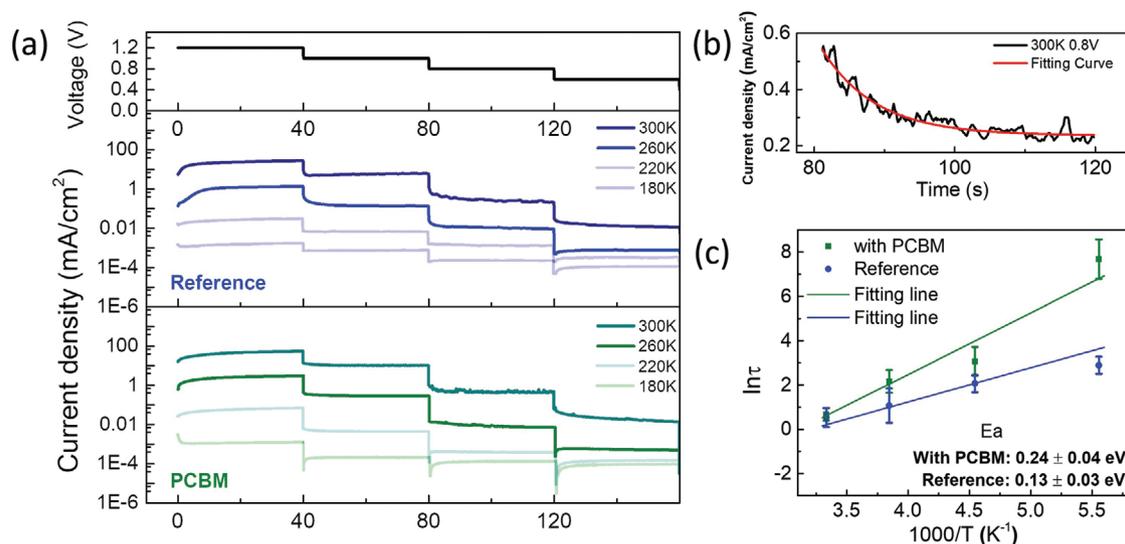
Figure 4. a) Temperature dependent chronoamperometric curve of reference device (blue) and PCBM (green) device, from 1.2 to 0.6 V with step of 0.2 V, each voltage lasts 40 s. The top part shows the applied voltage. b) Time dependent current density and fitting single exponential line at 0.8 V, 300 K. c) Activation energy of iodide ions in pure perovskite (reference) and perovskite on PCBM layer devices (PCBM device), respectively.

the perovskite layer. The detected PCBM may partially come from the dissolved PCBM in dimethylformamide during spin coating, as we make a detailed discussion in Figure S12, Supporting Information. Furthermore, PCBM molecules can also diffuse into perovskite film during film annealing. The evidence of fullerene diffusion through (amorphous/crosslinked[48] and crystalline[49]) polymer films has been demonstrated and was also suggested for perovskite films.[17] Our XPS results corroborate that PCBM molecules can readily diffuse into a ≈300 nm perovskite film at 105 °C within 75 min. This incorporation or interdiffusion into grain boundaries of the PCBM molecules seems to significantly reduce and hinder ionic migration.[50]

A further parameter which directly describes the viability for ion migration is the related activation energy. In a working perovskite solar cell, ions can migrate under an applied bias due to the prevalence of defects and may involve MA ions/vacancies[51,52] or iodine ions/vacancies.[53,54] Among them, the dominant moving species are iodine ions/vacancies.[55] The movement of these defects is in the form of hopping, also described as "jumping" in early days, between neighboring sites within the bulk with a rate Γ that can be expressed in an Arrhenius relation:[56]

$$\Gamma \propto \exp\left(\frac{-E_A}{k_B T}\right) \tag{2}$$

in which E_A is the activation energy, the energy required to move the defects from the equilibrium states to the neighbor sites in the bulk of perovskite. k_B and T are Boltzmann constant and absolute temperature, respectively.

Furthermore, we analyzed the activation barrier of ion migration of a pure perovskite film and another processed on a PCBM layer. This was done by applying voltage steps (0.2 V) to the device from 1.2 to 0.6 V and measuring the current evolution versus time, as shown in **Figure 4**a. The using voltage steps last 40s. The electrical current exhibits a decay-function

at each voltage step. A single exponential function $e^{-t/\tau}$ was used to evaluate the time constants as shown in Figure 4b. An Arrhenius plot shows a linear relationship between $\ln(\tau)$ and $1/T$ and suggests that the movement of ions is facilitated by a single hopping mechanism.[56] The constant of τ related with the "jumping rate" of ions Γ is used to describe the ionic migration within the bulk of the perovskite film.[57]

As shown in Figure 4c, it indicates that ions are moving faster in the perovskite film than the one on PCBM layer in all temperatures, consistent with the pervious PL microscopy observation. In the meantime, we note that the activation energy E_A of the pure perovskite is 0.13 ± 0.03 eV. This value agrees with a previous experiment and theoretical papers, ≈0.2 eV.[29,51,58] In direct comparison the meassured activation energy with a PCBM layer is 0.24 ± 0.04 eV, implying a higher energy required to drive these ions from equilibrium sites to the nearby sites in perovskite with the presence of PCBM molecules.

Taking account of the above experiments, the mechanism of suppression of hysteresis in PSCs incorporating with PCBM molecules becomes clearer. As proposed previously that the origin of the hysteresis in PSCs is due to the migration of iodine ions/vacancies. These ions are driven by the external field and accumulate at the interface between perovskite/ETL and HTL. This accumulation effectively enhances or decreases the built-in potential.[59] While, in PSCs incorporating with PCBM layer, PCBM molecules distribute within the bulk of perovskite film. Absorbed at perovskite defective sites along the grain boundaries, these PCBM molecules passivate these defect states, for example, iodine interstitials or iodide vacancies as we propose, decreasing or even halting ion migration within the perovskite film. It is possible that iodide ions from defects form strong bonding with PCBM molecules, by direct electron transfer from anions (iodide ions here).[15] In this respect, the iodide ions/defects are immobilized by tying up with the PCBM molecules in the bulk of perovskite. Alternatively, PCBM molecules only form a physical hindrance for
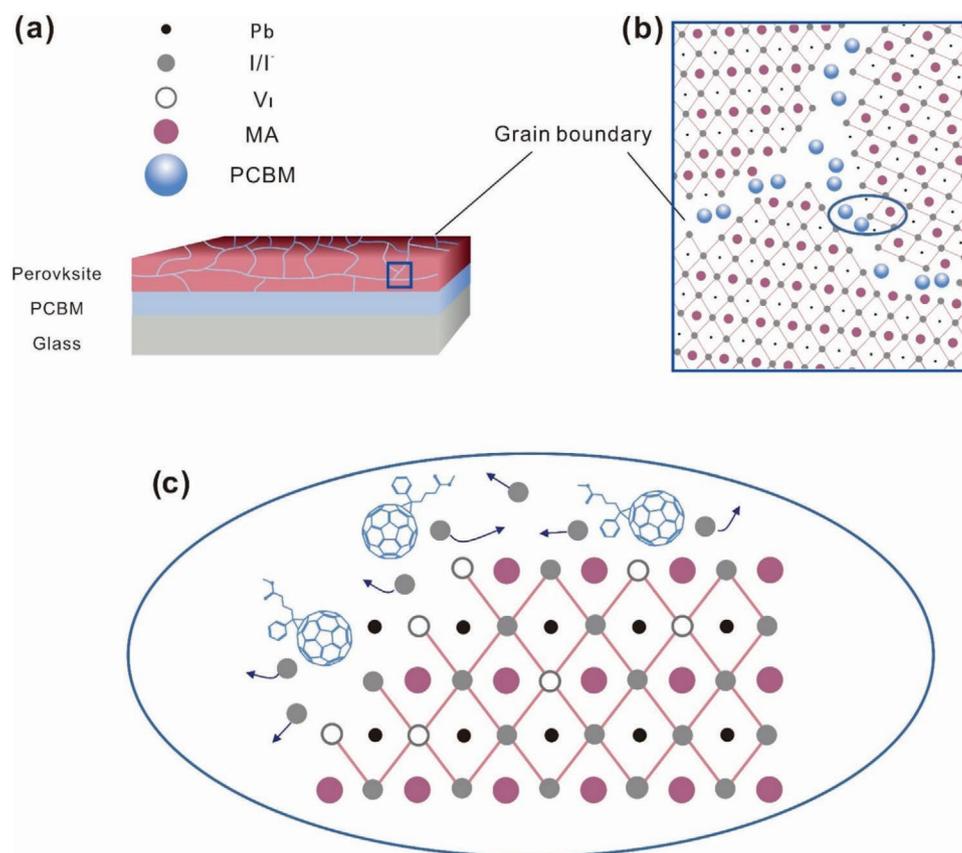
**ADVANCED
SCIENCE NEWS**
www.advancedsciencenews.com

**ADVANCED
FUNCTIONAL
MATERIALS**
www.afm-journal.de

Figure 5. Schematic diagram for the PCBM passivating iodide ion related defects in perovskite materials, particularly in the vicinity of grain boundary. a) Schematic of a perovskite film deposited on PCBM layer. b) Zoom in image of the rectangle area in (a), showing PCBM molecules penetrate into the grain boundary of perovskite layer. c) Zoomed-in image of circle area in (b), showing that PCBM molecules form hindrance of the iodide ions movement.

the ion migration or occupy some vacancy space, as displayed in **Figure 5**c. As a consequence, the moving defect density in perovskite reduces and the hysteresis is significantly suppressed due to the reduction of ionic migration.

For the PPCBM inserted device, the joint fullerene molecules are difficult to diffuse through the perovskite bulk material. Thus, the suppression of hysteresis is not distinct in these devices. However, V_{oc} of these devices in forward scan and reverse scan yields no pronounced difference. The reason is that the mismatch of TiO_2/perovskite interface is weakened by the PPCBM layer.[60] The interfacial barrier is hard to form at this contact and thus the change of the built-in potential is tiny. The ionic migration still exists in this perovskite/PPCBM bilayer system and so we observed a clear S-shape curve in forward scan direction.

It is necessary to note that apart from iodide ions, methylammonium (MA^+) ions may play a role in the hysteresis and degradation of perovskites.[52,61] The interaction between PCBM and MA^+ as well as characterization of MA^+ migration, however, are still not clearly elucidated. In addition, more and more evidences offer to present the critical role of grain boundary in the ion migration. However, due to resolution limitation of PL imaging microscopy, which is in ≈μm scale, it is difficult to directly explore the ion motion in the vicinity of grain boundary in our perovskite films (with grain size ≈100 nm). In the following experiment, by investigating perovskite films with various sizes,

it is possible to reveal the influence of grain boundary or even directly visualize the migration of ions in the grain boundary.

Our study also provides prospects for addressing the hysteresis problem in perovskite light-emitting diodes (LEDs), which is also much of concern.[62] Reducing defect/ion accumulation at perovskite/external contacts can increase the device stability as it has been demonstrated with the help of 2D or low-dimensional layered perovskites.[63] PCBM, however, may have to be used with care in LED devices as PCBM can greatly quench the emission of LEDs. Immobile (i.e., polymerized) derivatives, instead may become of great interest as PSC/ETL interlayers.

3. Conclusion

In summary, the comparison of PSCs using PCBM and PPCBM layer reveals that diffusion of PCBM molecules into grain boundaries of a polycrystalline perovskite film takes place and plays a significant role in the suppression of hysteresis in $J–V$ curve. By employing PL imaging microscopy, we directly in situ visualize and parameterize the ionic migration under external electrical fields. The ionic mobility is reduced by one order of magnitude, and temperature dependent chronoamperometric measurements show that the activation energy increases with the presence of PCBM molecules. Accounting for these results, we close with a proposed mechanism in the suppression of

hysteresis in PSCs with PCBM layer. PCBM molecules immobilize the iodine ions or vacancies in the bulk of the perovskite layer, reducing the impact of modulation of internal field/interfacial barriers under the external electrical field. This finding will pave paths to the improvement on the device stability and better performance. We reiterate that especially grain boundaries are responsible for an effective ion/vacancy migration which can be impeded through efficient passivation.

4. Experimental Section

Sample Preparation: CH_3NH_3I (MAI) was purchased from Dyesol company, Spiro-OMeTAD was purchased from Merck company, all the other chemicals were purchased from Sigma-Aldrich and were used as received without further purification. For $CH_3NH_3PbI_{3-x}Cl_x$ precursor solution, CH_3NH_3I, and $PbCl_2$ were dissolved in anhydrous Dimethylformamide at 3:1 molar ratio. Preparation of Spiro-OMeTAD solution: 72.3 mg Spiro-OMeTAD was dissolved in 1 mL chlorobezene with an additive of 43.2 µL 4-tert-butylpyridine. After that, 26.3 µL lithium bis(trifluoromethane)sulfonimide solution (520 mg mL^{-1} in acetonitrile) was added.

Fluorine-doped tin oxide (F:SnO$_2$) coated glass was patterned by Zn power and HCl solution. FTO glasses were washed successively with acetone, 2% hellmanex diluted in deionized water, deionized water, and isopropanol for 10 min each. A compact TiO_2 layer was deposited by spraying a solution of titanium diisopropoxide bis(acetylacetonate) (0.6 mL) in ethanol (21.4 mL) at 450 °C for 90 min in ambient atmosphere. The PCBM and PPCBM layer thicknesses were optimized for best electronic performance. For PCBM a 10 mg mL^{-1} solution in chlorobenzene was spin-coated at 3000 rpm for 30 s. After 10 min annealing at 100 °C, $CH_3NH_3PbI_{3-x}Cl_x$ perovskite solution was spin-coated on the PCBM layer at 3000 rpm for 60 s. For the devices using PPCBM, 5 mg mL^{-1} PPCBM in 1,2-dichlorobenzene was spin-coated at 2000 rpm for 30s. Following that, the $CH_3NH_3PbI_{3-x}Cl_x$ perovskite solution was spin-coated on this PCBM layer at 3000 rpm for 60s. After drying in a nitrogen glovebox for 30 min, the as-spun films were annealed at 105 °C for 1h15min on a hotplate. Subsequently, the hole transport layer (Spiro-OMeTAD solution) was deposited by spin-coating at 4000 rpm for 30 s. The device fabrication steps above were carried out in a nitrogen filled glovebox. After this, devices were transported to a dry box and stored there overnight enabling Spiro-OMeTAD oxidation. Finally, a 70 nm Au electrode was deposited by thermal evaporation in a chamber with a pressure of 1×10^{-6} mbar. The structure of the fabricated solar cell is FTO/TiO$_2$/perovskite/Spiro-OMeTAD/Au or FTO/TiO$_2$/PCBM or PPCBM/perovskite/Spiro-OMeTAD/Au.

Perovskite films for PL imaging microscopy and XPS are prepared as follows: The glass substrates were cleaned using an ultrasound bath with acetone for 5 min and another 5 min in isopropanol. After treatment with O$_3$ plasma, the perovskite precursor solution was spin coated on the substrates in a N$_2$ glove box. For perovskite PCBM bulk heterojunction devices, the perovskite precursor solution was mixed together the with PCBM solution with molar ratio Pb/PCBM = 500:1. For the perovskite/PCBM bilayer and perovskite/PPCBM devices, the perovskite film was directly deposited on the PCBM layer or PPCBM layer. All the films were annealed at 105 °C for 1 h 15 min. For PL imaging microscopy, in order to apply electrical field, lateral configured gold electrodes were evaporated on top of these films using a shadow mask. The distance between parallel electrodes was 200 µm and the interdigitating electrode geometry provided a ratio between channel width W and length L, W/L of 500. In the end, to protect the film from the oxygen and water, a 40 mg mL^{-1} poly(methyl methacrylate) (PMMA) solution dissolved in butyl acetate (anhydrous, 99%) was spin-coated at speed of 2000 rpm for 60 s.

J–V Measurement of Device: J–V measurements were carried out within inert environment using a Keithley 2400 source measure unit under 100 mW cm^{-2} illumination from an AM 1.5 solar simulator (Oriel company). The active area of 4 and 9 mm^2 were defined by the overlap of a black mask aperture area, the FTO and the evaporated top electrode. The light intensity was calibrated by a Si detector. No biasing process was applied prior to the scanning, we scanned from 1.2 to −0.1 V and then measured the reverse scanning continuously. The scanning speed is 0.8 V s^{-1} and each step was 0.01 V. Number of power line cycles (NPLC) was 0.1.

PL Imaging Microscopy: The setup of PL microscope is shown in detail in Figure S4, Supporting Information. The excitation source was a white light LED and it was combined with a dichroic mirror and a PL filter (HC 440 SP, AHF analysentechnik AG) in the excitation beam path. There was another filter (HC-BS 484, AHF analysentechnik AG) for the emitted PL signal from the sample. As a result, the wavelength of excitation beam was up to 440 nm and the emission signal comes to detector was above 490 nm. All the PL images were recorded by a CCD camera (Pco. Pixel fly, PCO AG) with an exposure time of 200 ms. For in situ electric measurement, samples were fixed on the microscope table and regions between Au electrodes were focused. An electric field was applied between the Au electrodes, simultaneously PL images were captured. The applied electric field varied from 5 to 40 V.

XPS Characterization: All the XPS measurements were carried with a PHI 5000 VersaProbe III system. An Al Kα excitation source was used (hν = 1486.6 eV) at a pass energy of 55 eV. A gas cluster ion beam (GCIB) forming clusters of ≈2500 Argon atoms was used to sputter the film step by step with a sputtering energy of 10 kV 30 nA and a duration of 0.5 min of each cycle.

Temperature Dependent Chronoamperometric Measurements: For temperature dependent J–V curves measurement, the samples were put into a continuous flow cryostat (Oxford Instruments, Optistat CF). PSCs (with and without PCBM layer) with effective area 4 mm^2 were measured in different temperatures (180, 220, 260, and 300°K) without light illumination. Step-wise voltage was applied to the cell from 1.2 to 0.6 V with the step of −0.2 V. The corresponding current density was recorded per microsecond.

Supporting Information

Supporting Information is available from the Wiley Online Library or from the author.

Acknowledgements

Conflict of Interest

The authors declare no conflict of interest.

Keywords

**ADVANCED
SCIENCE NEWS**

www.advancedsciencenews.com

**ADVANCED
FUNCTIONAL
MATERIALS**

www.afm-journal.de

[1] A. Kojima, K. Teshima, Y. Shirai, T. Miyasaka, *J. Am. Chem. Soc.* **2009**, *131*, 6050.

[2] D. P. Nenon, J. A. Christians, L. M. Wheeler, J. L. Blackburn, E. M. Sanehira, B. Dou, M. L. Olsen, K. Zhu, J. J. Berry, J. M. Luther, *Energy Environ. Sci.* **2016**, *9*, 2072.

[3] D. Luo, W. Yang, Z. Wang, A. Sadhanala, Q. Hu, R. Su, R. Shivanna, G. F. Trindade, J. F. Watts, Z. Xu, T. Liu, K. Chen, F. Ye, P. Wu, L. Zhao, J. Wu, Y. Tu, Y. Zhang, X. Yang, W. Zhang, R. H. Friend, Q. Gong, H. J. Snaith, R. Zhu, *Science* **2018**, *360*, 1442.

[4] F. Zhang, D. Bi, N. Pellet, C. Xiao, Z. Li, J. J. Berry, S. M. Zakeeruddin, K. Zhu, M. Grätzel, *Energy Environ. Sci.* **2018**, *11*, 3480.

[5] Z. Wang, Q. Lin, F. P. Chmiel, N. Sakai, L. M. Herz, H. J. Snaith, *Nat. Energy* **2017**, *2*, 17135.

[6] S. Ravishankar, S. Gharibzadeh, C. Roldán-Carmona, G. Grancini, Y. Lee, M. Ralaiarisoa, A. M. Asiri, N. Koch, J. Bisquert, M. K. Nazeeruddin, *Joule* **2018**, *2*, 788.

[7] W. Tress, N. Marinova, T. Moehl, S. M. Zakeeruddin, M. K. Nazeeruddin, M. Grätzel, *Energy Environ. Sci.* **2015**, *8*, 995.

[8] H. J. Snaith, A. Abate, J. M. Ball, G. E. Eperon, T. Leijtens, N. K. Noel, S. D. Stranks, J. T.-W. Wang, K. Wojciechowski, W. Zhang, *J. Phys. Chem. Lett.* **2014**, *5*, 1511.

[9] R. Gottesman, L. Gouda, B. S. Kalanoor, E. Haltzi, S. Tirosh, E. Rosh-Hodesh, Y. Tischler, A. Zaban, C. Quarti, E. Mosconi, F. De Angelis, *J. Phys. Chem. Lett.* **2015**, *6*, 2332.

[10] S. Meloni, T. Moehl, W. Tress, M. Franckevičius, M. Saliba, Y. H. Lee, P. Gao, M. K. Nazeeruddin, S. M. Zakeeruddin, U. Rothlisberger, M. Graetzel, *Nat. Commun.* **2016**, *7*, 10334.

[11] C. Li, S. Tscheuschner, F. Paulus, P. E. Hopkinson, J. Kießling, A. Köhler, Y. Vaynzof, S. Huettner, *Adv. Mater.* **2016**, *28*, 2446.

[12] C. Li, A. Guerrero, Y. Zhong, A. Gräser, C. A. M. Luna, J. Köhler, J. Bisquert, R. Hildner, S. Huettner, *Small* **2017**, *13*, 1701711.

[13] L. Bertoluzzi, R. A. Belisle, K. A. Bush, R. Cheacharoen, M. D. McGehee, B. C. O'Regan, *J. Am. Chem. Soc.* **2018**, *140*, 12775.

[14] A. Oranskaia, J. Yin, O. M. Bakr, J.-L. Brédas, O. F. Mohammed, *J. Phys. Chem. Lett.* **2018**, *9*, 5474.

[15] J. Xu, A. Buin, A. H. Ip, W. Li, O. Voznyy, R. Comin, M. Yuan, S. Jeon, Z. Ning, J. J. McDowell, P. Kanjanaboos, J.-P. Sun, X. Lan, L. N. Quan, D. H. Kim, I. G. Hill, P. Maksymovych, E. H. Sargent, *Nat. Commun.* **2015**, *6*, 7081.

[16] F. Zhang, W. Shi, J. Luo, N. Pellet, C. Yi, X. Li, X. Zhao, T. J. S. Dennis, X. Li, S. Wang, Y. Xiao, S. M. Zakeeruddin, D. Bi, M. Grätzel, *Adv. Mater.* **2017**, *29*, 1606806.

[17] Y. Shao, Z. Xiao, C. Bi, Y. Yuan, J. Huang, *Nat. Commun.* **2014**, *5*, 5784.

[18] E. Bi, H. Chen, F. Xie, Y. Wu, W. Chen, Y. Su, A. Islam, M. Grätzel, X. Yang, L. Han, *Nat. Commun.* **2017**, *8*, 15330.

[19] K. Wojciechowski, S. D. Stranks, A. Abate, G. Sadoughi, A. Sadhanala, N. Kopidakis, G. Rumbles, C.-Z. Li, R. H. Friend, A. K.-Y. Jen, H. J. Snaith, *ACS Nano* **2014**, *8*, 12701.

[20] G. Xing, B. Wu, S. Chen, J. Chua, N. Yantara, S. Mhaisalkar, N. Mathews, T. C. Sum, *Small* **2015**, *11*, 3606.

[21] N. J. Jeon, J. H. Noh, W. S. Yang, Y. C. Kim, S. Ryu, J. Seo, S. Il Seok, *Nature* **2015**, *517*, 476.

[22] H. Tsai, W. Nie, J. C. Blancon, C. C. Stoumpos, R. Asadpour, B. Harutyunyan, A. J. Neukirch, R. Verduzco, J. J. Crochet, S. Tretiak, L. Pedesseau, J. Even, M. A. Alam, G. Gupta, J. Lou, P. M. Ajayan, M. J. Bedzyk, M. G. Kanatzidis, A. D. Mohite, *Nature* **2016**, *536*, 312.

[23] R. S. Sanchez, V. Gonzalez-Pedro, J. W. Lee, N. G. Park, Y. S. Kang, I. Mora-Sero, J. Bisquert, *J. Phys. Chem. Lett.* **2014**, *5*, 2357.

[24] X. Cao, Y. Li, C. Li, F. Fang, Y. Yao, X. Cui, J. Wei, *J. Phys. Chem. C* **2016**, *120*, 22784.

[25] M. Hufnagel, M.-A. Muth, J. C. Brendel, M. Thelakkat, *Macromolecules* **2014**, *47*, 2324.

[26] M. Hufnagel, M. Thelakkat, *J. Polym. Sci., Part B: Polym. Phys.* **2016**, *54*, 1125.

[27] J. M. Frost, K. T. Butler, F. Brivio, C. H. Hendon, M. van Schilfgaarde, A. Walsh, *Nano Lett.* **2014**, *14*, 2584.

[28] X. Wu, M. T. Trinh, D. Niesner, H. Zhu, Z. Norman, J. S. Owen, O. Yaffe, B. J. Kudisch, X.-Y. Zhu, *J. Am. Chem. Soc.* **2015**, *137*, 2089.

[29] C. Li, S. Tscheuschner, F. Paulus, P. E. Hopkinson, J. Kießling, A. Köhler, Y. Vaynzof, S. Huettner, *Adv. Mater.* **2016**, *28*, 2446.

[30] D. A. Jacobs, Y. Wu, H. Shen, C. Barugkin, F. J. Beck, T. P. White, K. Weber, K. R. Catchpole, *Phys. Chem. Chem. Phys.* **2017**, *19*, 3094.

[31] C. Li, A. Guerrero, Y. Zhong, S. Huettner, *J. Phys.: Condens. Matter* **2017**, *29*, 193001.

[32] W. Tress, *J. Phys. Chem. Lett.* **2017**, *8*, 3106.

[33] P. Lopez-Varo, J. A. Jiménez-Tejada, M. García-Rosell, S. Ravishankar, G. Garcia-Belmonte, J. Bisquert, O. Almora, *Adv. Energy Mater.* **2018**, *8*, 1702772.

[34] Y. Deng, Z. Xiao, J. Huang, *Adv. Energy Mater.* **2015**, *5*, 1500721.

[35] S. T. Birkhold, J. T. Precht, H. Liu, R. Giridharagopal, G. E. Eperon, L. Schmidt-Mende, X. Li, D. S. Ginger, *ACS Energy Lett.* **2018**, *3*, 1279.

[36] Y. Yamada, T. Nakamura, M. Endo, A. Wakamiya, Y. Kanemitsu, *J. Am. Chem. Soc.* **2014**, *136*, 11610.

[37] S. Chen, X. Wen, R. Sheng, S. Huang, X. Deng, M. A. Green, A. Ho-Baillie, *ACS Appl. Mater. Interfaces* **2016**, *8*, 5351.

[38] D. W. de Quilettes, S. M. Vorpahl, S. D. Stranks, H. Nagaoka, G. E. Eperon, M. E. Ziffer, H. J. Snaith, D. S. Ginger, *Science* **2015**, *348*, 683.

[39] C. Li, A. Guerrero, S. Huettner, J. Bisquert, *Nat. Commun.* **2018**, *9*, 5113.

[40] Y. Zhong, C. A. M. Luna, R. Hildner, C. Li, S. Huettner, *APL Mater.* **2019**, *7*, 041114.

[41] E. Bandiello, J. Ávila, L. Gil-Escrig, E. Tekelenburg, M. Sessolo, H. J. Bolink, *J. Mater. Chem. A* **2016**, *4*, 18614.

[42] E. Mosconi, F. De Angelis, *ACS Energy Lett.* **2016**, *1*, 182.

[43] X. Wu, M. T. Trinh, D. Niesner, H. Zhu, Z. Norman, J. S. Owen, O. Yaffe, B. J. Kudisch, X.-Y. Zhu, *J. Am. Chem. Soc.* **2015**, *137*, 2089.

[44] J. M. Lownsbury, J. C. Sharp, E. J. Mann, C. T. Campbell, *J. Phys. Chem. C* **2015**, *119*, 18444.

[45] R. P. Vasquez, R. A. Brain, D. Ross, N. Yeh, *Surf. Sci. Spectra* **1992**, *1*, 242.

[46] S. Olthof, K. Meerholz, *Sci. Rep.* **2017**, *7*, 40267.

[47] Q. Sun, P. Fassl, D. Becker-Koch, A. Bausch, B. Rivkin, S. Bai, P. E. Hopkinson, H. J. Snaith, Y. Vaynzof, *Adv. Energy Mater.* **2017**, *7*, 1700977.

[48] F. Fischer, T. Hahn, H. Bässler, I. Bauer, P. Strohriegl, A. Köhler, *Adv. Funct. Mater.* **2014**, *24*, 6172.

[49] B. Watts, W. J. Belcher, L. Thomsen, H. Ade, P. C. Dastoor, *Macromolecules* **2009**, *42*, 8392.

[50] Y. Yuan, J. Huang, *Acc. Chem. Res.* **2016**, *49*, 286.

[51] J. M. Azpiroz, E. Mosconi, J. Bisquert, F. De Angelis, *Energy Environ. Sci.* **2015**, *8*, 2118.

[52] Y. Yuan, J. Chae, Y. Shao, Q. Wang, Z. Xiao, A. Centrone, J. Huang, *Adv. Energy Mater.* **2015**, *5*, 1500615.

[53] T. Y. Yang, G. Gregori, N. Pellet, M. Grätzel, J. Maier, *Angew. Chem., Int. Ed.* **2015**, *54*, 7905.

[54] Y. Yuan, Q. Wang, Y. Shao, H. Lu, T. Li, A. Gruverman, J. Huang, *Adv. Energy Mater.* **2016**, *6*, 1501803.

[55] C. Eames, J. M. Frost, P. R. F. Barnes, B. C. O'Regan, A. Walsh, M. S. Islam, *Nat. Commun.* **2015**, *6*, 7497.

[56] G. H. Vineyard, *J. Phys. Chem. Solids* **1957**, *3*, 121.

[57] C. Wert, C. Zener, *Phys. Rev.* **1949**, *76*, 1169.

[58] H. Yu, H. Lu, F. Xie, S. Zhou, N. Zhao, *Adv. Funct. Mater.* **2016**, *26*, 1411.

[59] Y. Zhang, M. Liu, G. E. Eperon, T. C. Leijtens, D. McMeekin, M. Saliba, W. Zhang, M. De Bastiani, A. Petrozza, L. M. Herz, M. B. Johnston, H. Lin, H. J. Snaith, *Mater. Horiz.* **2015**, *2*, 315.

[60] G. Garcia-Belmonte, J. Bisquert, *ACS Energy Lett.* **2016**, *1*, 683.

[61] T. Leijtens, E. T. Hoke, G. Grancini, D. J. Slotcavage, G. E. Eperon, J. M. Ball, M. De Bastiani, A. R. Bowring, N. Martino, K. Wojciechowski, M. D. McGehee, H. J. Snaith, A. Petrozza, *Adv. Energy Mater.* **2015**, *5*, 1500962.

[62] Z.-K. Tan, R. S. Moghaddam, M. L. Lai, P. Docampo, R. Higler, F. Deschler, M. Price, A. Sadhanala, L. M. Pazos, D. Credgington, F. Hanusch, T. Bein, H. J. Snaith, R. H. Friend, *Nat. Nanotechnol.* **2014**, *9*, 687.

[63] C. Li, N. Wang, A. Guerrero, Y. Zhong, H. Long, Y. Miao, J. Bisquert, J. Wang, S. Huettner, *J. Phys. Chem. Lett.* **2019**, *10*, 6857.

1908920 (9 of 9)